Heisenberg-limited quantum interferometry with multiphoton-subtracted twin beams

Miller Eaton ©,* Rajveer Nehra ©, Aye Win, and Olivier Pfister ©

Department of Physics, University of Virginia, 382 McCormick Road, Charlottesville, Virginia 22903, USA

We propose a Heisenberg-limited quantum interferometer whose input is twin optical beams from which one or more photons have been indistinguishably subtracted. Such an interferometer can yield Heisenberg-limited performance while at the same time giving a direct fringe reading, unlike for the twin-beam input of the Holland-Burnett interferometer. We propose a feasible experimental realization using a photon-number correlated source, such as nondegenerate parametric down-conversion, and perform realistic analyses of performance in the presence of loss and detector inefficiency.

I. INTRODUCTION

A general interferometer, typified by the Mach-Zehnder interferometer (MZI) of Fig. 1, measures the phase difference between two propagation paths by probing them with mutually coherent waves. From a purely undulatory standpoint, a sure way of ensuring such mutual coherence is to split an initial wave into two waves, for example by use of a beam splitter. However, the unitarity of quantum evolution mandates that any two-wave-output unitary have a two-mode input as well, rather than a classical, single-mode input. Thus, the quantum description of a "classical" interferometer must feature an "idle" vacuum field in addition to the initial wave, and the quantum fundamental limit of interferometric measurements is then dictated by the corpuscular statistics of the interference between the two inputs of the beam splitter (Fig. 1). In a classical interferometer, the vacuum fluctuations at the idle input port limit the phase difference sensitivity between the two interferometer arms to the quantum limit of classical interferometry [1], the input beam splitter's shot-noise limit (SNL) [2]

$$\Delta\phi_{\rm SN} \sim \langle N \rangle^{-\frac{1}{2}}, \tag{1}$$

where ϕ is the phase difference to be measured and $N = N_a + N_b$ is the total photon number operator. This limit is that of phase noise *inside* the interferometer and has nothing to do with, say, the single-mode properties of a coherent-state (e.g., laser) input $|\alpha\rangle$ of photon-number deviation $\Delta N = |\alpha| = \langle N \rangle^{1/2}$ and phase deviation [5] $\Delta\theta \sim \langle N \rangle^{-1/2}$ *before* the interferometer. In fact, Caves showed that a Fock-state input $|n\rangle$, for which $\Delta N = 0$ and hence $\Delta\theta \to \infty$, still yields the SNL of Eq. (1) [1].

When both input modes of the interferometer are properly "quantum engineered," one can, in principle, reach the ultimate limit, called the Heisenberg limit (HL),

$$\Delta\phi_H \sim \langle N \rangle^{-1}, \tag{2}$$

which can clearly be many orders of magnitude lower than the SNL when $\langle N \rangle \gg 1$. A recent comprehensive review of quantum interferometry can be found in Ref. [7]. The first quantum engineering proposal to break through the SNL was Caves's idea to replace the vacuum-state input with a squeezed vacuum [8], which has since been shown to optimize the quantum Cramér-Rao bound when the input field is a coherent state [9]. This was demonstrated experimentally [10,11] and is now the approach adopted for high-frequency signals (above the standard quantum limit) in gravitational-wave detectors [12,13]. Many other approaches have been investigated [14,15], such as twin beams [16–21], NOON states [22–26], or two-mode squeezed (TMS) states. These different schemes were recently compared in terms of the quantum Cramér-Rao bound on their phase sensitivity [27].

It is important to recall here the essential result of Escher, de Matos Filho, and Davidovich: operating a realistic, i.e., lossy, interferometer at the HL requires losses to be no greater than $\langle N \rangle^{-1}$ [28]; i.e., the grand total of the loss can never exceed one photon, on average. This result had been obtained earlier by Pooser and Pfister in the particular case of Holland-Burnett interferometry [29]: using Monte Carlo simulations for up to $n = 10\,000$ photons, it was shown that the phase error of a nonideal Holland-Burnett interferometer scales with the HL if the losses are of the order of n^{-1}, and that larger losses degrade the scaling to a limit proportional to the SNL of $N^{-1/2}$, staying sub-SNL as long as photon correlations are present in the twin Fock input. This is consistent with the general result of Escher, de Matos Filho, and Davidovich for phase estimation [28]. Additionally, in the case of loss, optimal input states have been numerically calculated whose form generally depends on the interferometric efficiency and average photon-number input [30].

A direct consequence is that, if the total photon number is too large, ultimate-sensitivity interferometry cannot be Heisenberg limited in the current state of technology: the most sensitive classical interferometer to date, the Laser Interferometer Gravitational-wave Observatory (LIGO), before the introduction of squeezed light boasted $\Delta\phi_{\rm SN} \sim 10^{-11}$ rad and is shot-noise limited in some spectral regions, therefore

*me3nq@virginia.edu

TABLE I. Characteristics and performance of different input states, except the NOON state which is a state specified *inside* the interferometer. The phase error $\Delta\phi$ is the quantum Cramér-Rao bound [27]. The state whose use we propose in this paper is the last one.

	Input* state	Ref.	(i) $\Delta\phi$		(ii) Fringe $\langle N_a - N_b \rangle$	(iii) $\langle N \rangle \gg 1$?
1	$\lvert n \rangle_a \lvert 0 \rangle_b$	[1]	$\dfrac{1}{\sqrt{n}}$	SNL	$n\cos\phi$	yes
2	$\lvert \alpha \rangle_a \lvert 0 \rangle_b$	[1]	$\dfrac{1}{\sqrt{\langle N \rangle}} = \dfrac{1}{\lvert \alpha \rvert}$	SNL	$\lvert \alpha \rvert^2 \cos\phi$	yes
3	$\lvert \alpha \rangle_a \lvert 0, r \rangle_b$	[8]	$\simeq \dfrac{e^{-r}}{\lvert \alpha \rvert}$	sub-SNL	$\lvert \alpha \rvert^2 \cos\phi$	yes
4	$\lvert n \rangle_a \lvert n \rangle_b$	[16]	$\dfrac{1}{\sqrt{2n(n+1)}}$	HL	0	yes [20]
5	$\lvert n \rangle_a \lvert n-1 \rangle_b$	[27]	$\dfrac{1}{\sqrt{2n^2 - 1}}$	HL	$\dfrac{1}{2}\cos\phi$	possible
6*[a]	$\dfrac{1}{\sqrt{2}}(\lvert n \rangle_a \lvert 0 \rangle_b + \lvert 0 \rangle_a \lvert n \rangle_b)$	[22,23]	$\dfrac{1}{n}$	HL	$\sim \cos(n\phi)$[b]	unknown
7	$\dfrac{1}{\sqrt{2}}(\lvert n \rangle_a \lvert n \rangle_b + \lvert n+1 \rangle_a \lvert n-1 \rangle_b)$	[14]	$\dfrac{1}{\sqrt{2n(n+1)-1}}$	HL	$\dfrac{\cos\phi}{2} - \dfrac{\sin\phi}{4}\sqrt{n(n+2)}$	unknown
8	$\displaystyle\sum_{k=0}^{Z} c_k \lvert n-Z+k \rangle_a \lvert n-k \rangle_b$		$\simeq \dfrac{\sqrt{Z}}{n}$	HL	$\sim \dfrac{n}{2}\sin\phi$	possible

[a]NOON state, which is specified *inside* the interferometer.
[b]The fringe signal for the NOON state requires n-photon detection.

featuring $\langle N \rangle \sim 10^{22}$ photons. While a Heisenberg-limited version of LIGO would only require $\langle N \rangle \sim 10^{11}$ photons to reach the same sensitivity, it would also require an unrealistic loss level of 10^{-11}, the optical coatings on LIGO's mirrors "only" reaching already remarkable sub-ppm loss levels [31].

However, the maximally efficient use of photons by Heisenberg-limited interferometry can still be interesting provided we take into account this constraint of an ultimate loss level of 10^{-6}. At this level, a 1064-nm interferometer with (arbitrarily chosen) 10-ms measurements would be allowed to reach the 10^6-photon HL of 1 μrad with only 200 pW, whereas a classical interferometer would need 10^{12} photons, i.e., 200 μW, to have its SNL at 1 μrad. This can be of interest in situations where low light levels are beneficial, such as phase imaging of living biological tissue.

A. SU(2) interferometry

In order to motivate the approach of this paper, we review and compare and contrast some different quantum-enhanced sensing proposals in Table I. The key points we examine are (i) whether the input state enables performance at the HL, (ii) whether a direct interference fringe is observable, and (iii) whether the $\langle N \rangle \gg 1$ regime is experimentally accessible. As will be shown, the new input state we propose in this paper is the only one that fulfills all three criteria.

The first two cases are interferometry with the vacuum field in one beam-splitter input port, leading to no quantum enhancement.

The third case makes use of Caves's squeezed input [8] into the previously unused port of the beam splitter. This benefits from mature, high-level laser and quantum optics technology, with large average photon numbers from well-stabilized lasers [32]. Case 3 benefits from the recent 15-dB squeezing record [33], but it does require that the phase difference between

the squeezed state and the coherent state be controlled [34]. The gravitational-wave observatories of Advanced LIGO, Advanced VIRGO, and GEO600 all currently utilize squeezed light to improve sensitivity [35–37], and Advanced LIGO will soon implement frequency-dependent squeezing to improve sensitivity over a larger bandwidth [38].

Case 4 in Table I is the twin Fock-state input first proposed by Holland and Burnett [16], and which is implementable, to a good approximation, with large photon numbers by using an optical parametric oscillator above threshold [20,21,39–41]. The input density operator is then of the form, in the absence of losses,

$$\rho = \sum_{n,n'} \rho_{n,n'} \lvert nn \rangle \langle n'n' \rvert, \tag{3}$$

which can be a pure state ($\rho_{n,n'} \mapsto \rho_n \rho_{n'}^*$), e.g., the TMS state emitted by a lossless optical parametric oscillator (OPO) below threshold, or it can be a general statistical mixture as emitted by a lossless OPO above threshold [42]. It thus also benefits from the same mature OPO-based squeezing technology, with a record 9.7 dB reduction on the intensity-difference noise [41]. Moreover, the phase difference between the twin beams is irrelevant (being actually very noisy from being antisqueezed) and thus need not be controlled before the interferometer. The generalized [43] Hong-Ou-Mandel [44] quantum interference responsible for twin beams breaking the SNL was demonstrated experimentally in an ultrastable phase-difference-locked OPO above threshold [20,45,46], with several milliwatts of continuous wave laser power.

An inconvenient feature of the Holland-Burnett scheme, however, is that the direct interference fringe disappears ($\langle N_a - N_b \rangle = 0$ in Table I), a property also shared by the classical input $\lvert \alpha \rangle_a \lvert \alpha \rangle_b$) in contrast to all previous cases for which the fringe signal is proportional to the total photon number. This inconvenience can be circumvented by the

use of Bayesian reconstruction of the probability distribution [16,18,29]. Although recently demonstrated for low photon numbers [47], this requires photon-number-resolved detection, which has yet to be experimentally accessible for large photon numbers. Another workaround is to use the variance of the photon-number difference, which is sensitive to ϕ [17] but whose signal-to-noise ratio is bounded by $\sqrt{2}$ [18]. Another idea is to use a heterodyne signal, which presents high visibility but is restricted to phase shifts ever closer to zero as the squeezing increases [48]. This was demonstrated experimentally as heterodyne polarimetry 4.8 dB below the SNL [21].

Case 5 in Table I is a variant of the twin Fock state, the "fraternal" twin Fock state [27], which does provide a direct fringe signal which is Heisenberg limited, but the fringe signal is still extremely small as it does not scale with the input photon number. Recently, other variants of this state in the family $|n\rangle_a|m\rangle_b$ have shown better performance than Holland-Burnett and NOON states in the presence of loss [49].

Case 6 stands out for several reasons. The NOON state refers not to an interferometer input state but to a state inside the Mach-Zehnder interferometer [22,23]. While it yields performance at the HL, its experimental generation is experimentally inaccessible for $n \gg 1$; previous experimental realizations have used postselected outcomes for $n = 3$ [24] and 4 [25], a method which fails to scale up to large photon numbers, though a more scalable method using coherent-state displacement was also demonstrated [26]. Furthermore, NOON states are extremely vulnerable to loss [50], although experimental efforts have attempted to sidestep the issue by using more loss-tolerant techniques [51]. Last but not least, the use of a NOON state with n photons requires n-photon detection, which is currently inaccessible in optics experiments with $n \gg 1$ (but may be easier to reach in atomic spectroscopy [22]).

Case 7 is the theoretical proposal of Yurke, McCall, and Klauder [14]. It features both performance at the HL and a strong fringe signal, but an experimental realization has yet to be determined.

Case 8 features the input proposed in this paper; it is the only one of the table that features HL performance and a clear interference fringe signal, and is experimentally feasible with demonstrated technology for large photon numbers. The state can be generated by using bright twin beams from which one or multiple photons have been coherently subtracted.

In addition to the above cases, photon subtraction has been suggested to be used in other interferometry schemes, such as interfering a coherent state and photon-subtracted squeezed vacuum [52] or subtracting a photon from each mode of a TMS state [53] (*distinguishable* subtraction, unlike what we propose here), but these schemes would require either a parity measurement or large photon-number resolving (PNR) measurements for end detection, both of which are currently unfeasible for large photon numbers and will be discussed further in Sec. VII. As will be demonstrated, our method can make use of bright twin beams, thus scaling to large numbers of photons, and provides a directly measurable fringe with conventional photodiodes. As mentioned, the presence of a strong fringe mitigates the need for numerically intensive reconstruction of the measured distribution.

B. A note on SU(1,1) interferometry

We have to our knowledge covered many of the basic approaches to quantum-enhanced optical interferometry with SU(2)-based interferometers, but it is also important to mention SU(1,1) interferometry where the traditional passive beam splitters are replaced by nonlinear two-mode squeezers. These devices do not work with intensity difference measurements [54], but must instead rely on other techniques, such as parity detection, which requires a PNR detector and is highly susceptible to loss [55]. This weakness to loss can be mitigated by seeding the input with a coherent state [56] and the PNR detector can be replaced with a click detector [57], but in neither case will the detection sensitivity achieve the HL scaling. Alternatively, both the full SU(1,1) interferometer and a truncated version [58] can reach the HL with homodyne detection. Sensitivity below the SNL has been experimentally demonstrated [59] and this idea has been used to propose measuring angular displacement [60]. However, the use of homodyne detection on each mode means that the local oscillator phases on two auxiliary beams must be carefully controlled. Even if they are well phase locked, an overall additive phase inside the interferometer may be disguised as the differential phase we wish to measure with the traditional SU(2) interferometer. In fact, the use of dual homodyne detection in SU(1,1) interferometric devices actually lends them the ability to more generally detect displacements, which prompted Caves to propose renaming them SU(1,1) displacement sensors [61]. In this work, we suggest using a squeezer in Sec. V as part of the state generation process which is reminiscent of the nonlinearity present in SU(1,1) interferometry. However, this is just for convenience, as any twin-correlated source will work as stated in Sec. VI C. Squeezing has also been used postinterferometer as a means to amplify the quantum signal to a classical one before detection in order to mitigate problems with inefficient detection [62]. From this point on, we restrict our study to that of SU(2) interferometry.

This paper is organized as follows. In Sec. II, we introduce the Schwinger-spin representation and calculate the Cramér-Rao bound by way of the quantum Fisher information for our proposed state. Section III demonstrates that the Z-photon coherently subtracted twin-beam state has phase-sensitivity scaling with the HL when implemented with a traditional MZI. We then propose an experimental scheme to generate the desired state in Sec. IV and derive the result from a twin-beam input. Section V shows the results of numerical calculations when all approximations are disregarded, and Sec. VI discusses practical considerations of loss, detection imperfections, and the use of click detectors in place of PNR detectors during state generation. Section VII compares cases with distinguishable subtraction in place of coherent subtraction, and then we conclude.

II. QUANTUM FISHER INFORMATION

The Fisher information is a well-known parameter that provides a means to quantify the amount of information contained by a parametrized random variable, and the Cramér-Rao inequality formulates an upper bound on the precision of an estimator in terms of the Fisher information [63,64]. This

inequality has been extended to the quantum case [65], which is very useful in determining the bounds on the sensitivity for quantum interferometry given a specified input state [9], and is independent of the nature of the estimator. For a standard MZI, the estimator of interest is the phase difference between the two arms of the interferometer, for which the quantum Fisher information of a general pure input state is given by [9,66]

$$\mathcal{F} = \langle \psi_{in}| U_{\mathrm{BS}}^{\dagger} N_d^2 U_{\mathrm{BS}} |\psi_{in}\rangle - \langle \psi_{in}| U_{\mathrm{BS}}^{\dagger} N_d U_{\mathrm{BS}} |\psi_{in}\rangle^2, \quad (4)$$

where $U_{\mathrm{BS}} = \exp(\frac{i\pi}{4}(a^{\dagger}b + ab^{\dagger}))$ is a balanced beam splitter and $N_d = a^{\dagger}a - b^{\dagger}b$ is the photon number difference operator. For the sake of convenience, we adopt for our calculation the Schwinger-spin SU(2) representation [67] initially proposed by Yurke *et al.* for quantum interferometers [14]. A fictitious spin $\vec{J}$ is defined from a pair of bosonic modes (a, b) as

$$J_z = \tfrac{1}{2}(a^{\dagger}a - b^{\dagger}b), \quad (5)$$

$$J_x = \tfrac{1}{2}(a^{\dagger}b + ab^{\dagger}), \quad (6)$$

$$J_y = -\tfrac{i}{2}(a^{\dagger}b - ab^{\dagger}), \quad (7)$$

where a and b are the annihilation operators of each mode. These operators satisfy the canonical angular momentum commutation relations of the SU(2) algebra,

$$[J_i, J_j] = i\epsilon_{ijk}J_k. \quad (8)$$

The operator J_z represents the photon-number difference operator between the two modes whereas $J_{x,y}$ are interference terms. The ease of working with Schwinger operators is further simplified by noting that the common eigenstates of J_z and J^2, $|j, m\rangle$, take the form of two-mode Fock states:

$$|j, m\rangle = |n_a\rangle_a |n_b\rangle_b, \quad (9)$$

where we have

$$j = \tfrac{1}{2}(n_a + n_b), \quad (10)$$

$$m = \tfrac{1}{2}(n_a - n_b). \quad (11)$$

We can then see that the Fisher information can be expressed as

$$\mathcal{F} = 4 \langle \psi_{in}| e^{(-i\frac{\pi}{2}J_x)} J_z^2 e^{(i\frac{\pi}{2}J_x)} |\psi_{in}\rangle$$
$$- 4 \langle \psi_{in}| e^{(-i\frac{\pi}{2}J_x)} J_z e^{(i\frac{\pi}{2}J_x)} |\psi_{in}\rangle^2 \quad (12)$$

$$= 4 \langle \psi_{in}| J_y^2 |\psi_{in}\rangle - 4 \langle \psi_{in}| J_y |\psi_{in}\rangle^2 \quad (13)$$

$$= \langle (a^{\dagger}b - ab^{\dagger})^2 \rangle + \langle a^{\dagger}b - ab^{\dagger} \rangle^2. \quad (14)$$

This quantity is related to the phase estimation bound by

$$(\Delta\phi_d)^2 \geqslant \frac{1}{\mathcal{F}}. \quad (15)$$

It is important to note that $\Delta\phi_d$ is the general phase difference measurement whereas the quantum Fisher-limited phase error, i.e., when the inequality achieves equality, can be achieved for the correct estimator when ϕ deviates from an initially specified optimal value.

For an interferometry scheme using solely a coherent-state input, the Fisher information can be easily calculated

to yield exactly the expectation value of the input photon number, $\mathcal{F} = \langle N \rangle$. This leads to a maximum phase sensitivity of $\Delta\phi_d = \langle N \rangle^{-1/2}$, which is the well-known limit to interferometric measurement due to quantum noise with a classical input shown in Table I, case 2. In order to beat this limit, it becomes necessary to include something other than coherent states and vacuum as input, such as squeezed light addressed by case 3 of Table I. Although this will beat the $\langle N \rangle^{-1/2}$ scaling, it still cannot achieve the HL and has a maximum scaling of $\sim \langle N \rangle^{-2/3}$, which is only achievable with large squeezing ($\sim |\alpha|^{2/3}$ photons in the squeezed field for $|\alpha|^2$ photons in the coherent state) [1]. Because of this, reaching the HL requires the use of other types of quantum states. As a start, consider the simplest case of the final state in Table I (the $Z = 1$ case), the state given by

$$|\psi^{(i)}\rangle = A |n - 1\rangle_a |n\rangle_b + B |n\rangle_a |n - 1\rangle_b, \quad (16)$$

where $|A|^2 + |B|^2 = 1$. Calculating the quantum Fisher information for $\psi^{(i)}$ in Eq. (16) gives

$$\mathcal{F}^{(i)} = 2n^2 - 4n^2 \mathrm{Im}[A^*B] - 1, \quad (17)$$

which leads to the inequality

$$\left(\Delta\phi_d^{(i)}\right)^2 \geqslant \frac{1}{2n^2 - 1} \quad (18)$$

when $A = B = \frac{1}{\sqrt{2}}$. In general, it is possible to achieve the Cramér-Rao bound by judiciously choosing the ideal measurement scheme [68]. If the ideal measurement is physically realizable, such as photon-number difference or single-mode parity, Eq. (18) demonstrates that the maximum sensitivity of $\Delta\phi_d$ can achieve a Heisenberg-limited scaling of $\langle N \rangle^{-1}$.

We now consider the most general state with arbitrary Z:

$$|\psi\rangle = c_0 |n - Z\rangle_a |n\rangle_b + c_1 |n - Z + 1\rangle_a |n - 1\rangle_b$$
$$+ \cdots + c_Z |n\rangle_a |n - Z\rangle_b$$
$$= \sum_{k=0}^{Z} c_k |n - Z + k\rangle_a |n - k\rangle_b, \quad (19)$$

where some initial $|n\rangle_a |n\rangle_b$ has been subjected to a coherent Z-photon subtraction, where the Z photons could have been removed from either mode in any given combination. Derived in Appendix B, the Fisher information when all c_k are the same and the mean photon number of the state is much larger than the number of photons subtracted is determined to be

$$\mathcal{F} \stackrel{(i)}{=} \frac{N^2}{Z}, \quad (20)$$

where "(i)" represents the use of the condition that $N = 2n - Z \gg Z$. This leads to a bound on the phase sensitivity to be

$$(\Delta\phi_d)^2 \geqslant \frac{Z}{N^2}, \quad (21)$$

which shows the potential to achieve scaling that is proportional to HL. Although the bound given by the Fisher information is general, true interferometric performance is dependent upon the measurement scheme. We will now demonstrate that the class of states given by Eq. (19) follows the N^{-1} scaling in a realistic MZI implementation when subtracting the resultant photodetection currents, and will
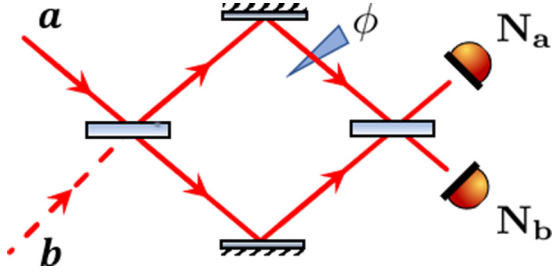
FIG. 1. A Mach-Zehnder interferometer with phase difference ϕ between two optical paths. Both beam splitters are balanced. Quantum splitting of input field a implies interference with the vacuum field b.

also yield a measurable interference fringe scaling with input photon number. From there, we will provide a feasible experimental scheme based on correlated twin beams and a single multiphoton subtraction event.

III. MZI IMPLEMENTATION SENSITIVITY

The above discussion demonstrated that the generalized photon-subtracted states are potentially viable for Heisenberg-limited interferometry as verified by the quantum Fisher information, but now it is important to ensure that the same $\langle N \rangle^{-1}$ scaling can be reached with a realistic implementation, such as subtracting photocurrents, and that there is a measurable fringe *also* scaling with $\langle N \rangle$ to ensure a sufficient signal above any electronics noise floor. The standard MZI is shown for reference in Fig. 1, where $\Delta\phi$ is the phase difference between the arms of the interferometer and the end detectors measured the respective mean photocurrents, N_a and N_b.

The input state, $|\psi\rangle_{ab}$, is transformed using the Schrödinger picture by the interferometer to

$$|\psi'\rangle_{ab} = U_{\text{BS}}^\dagger P_{\Delta\phi} U_{\text{BS}} |\psi\rangle_{ab}, \tag{22}$$

where $P_{\Delta\phi}$ applies the relative phase shift $\Delta\phi$. This is equivalent, in the Schwinger representation, to applying the rotations

$$|\psi'\rangle_{ab} = e^{-i\frac{\pi}{2}J_x} e^{i\phi J_z} e^{i\frac{\pi}{2}J_x} |\psi\rangle_{ab}. \tag{23}$$

However, in order to determine if there is a measurable fringe, it is necessary to find $\langle N_a - N_b \rangle$, which is much easier to find when working in the Heisenberg picture, as it simply corresponds to the transformed rotation operator, $\langle J_z' \rangle$, where any operator, O, is transformed by the MZI to become

$$O' = e^{-i\frac{\pi}{2}J_x} e^{-i\phi J_z} e^{i\frac{\pi}{2}J_x} O e^{-i\frac{\pi}{2}J_x} e^{i\phi J_z} e^{i\frac{\pi}{2}J_x}. \tag{24}$$

Using the transformation, we find

$$J_z' = \cos\phi J_z - \sin\phi J_x. \tag{25}$$

Making use of Eqs. (9)–(11), we can rewrite the state of interest from Eq. (19) in the Schwinger representation to be

$$|\psi\rangle = \sum_{m=-s}^{s} c_m |jm\rangle, \tag{26}$$

where $s = \frac{1}{2}Z$, $j = n - s$, and from this point forward we consider all coefficients real and symmetric such that

$$c_m^* = c_m = c_{-m}, \tag{27}$$

which is the case for the physical state as derived in Appendix A. Supposing condition (i) that the number of photons removed from the state by the subtraction process is considerably smaller than the number of photons remaining, i.e., $j \gg s$, the measurable fringe for the state in Eq. (26) is given by

$$\frac{j}{s}|\sin\phi| \overset{\text{(i,ii)}}{\leqslant} 2|\langle J_z'\rangle| \overset{\text{(i)}}{\leqslant} 2j|\sin\phi|, \tag{28}$$

with "(ii)" denoting the use of results from Appendix A 2 where we bound the closeness of neighboring coefficients c_m, c_{m+1} obtained from the experimental design. Equation (28) shows that there is a direct measurable fringe scaling with j. Now, in order to determine the phase sensitivity when using J_z' as a phase estimator, it is necessary to calculate the quantity

$$(\Delta\phi)^2 = \left[\Delta J_z' \left(\frac{\partial d}{\partial d\phi} \langle J_z' \rangle \right)^{-1} \right]^2. \tag{29}$$

Derived in Appendix B, $\Delta\phi$ takes on a minimum value about the angle $\phi = 0$, yielding an upper bound on the phase sensitivity of

$$\frac{\sqrt{s}}{j} \overset{\text{(i)}}{\leqslant} \Delta\phi_{\text{min}} \overset{\text{(i,ii)}}{\leqslant} \frac{2s^2}{j}. \tag{30}$$

We note again that s is a small number based on the number of photons subtracted, so it is simply a constant factor that does not affect scaling. Together, Eqs. (28) and (30) show that the general Z-photon subtracted state has sensitivity proportional to the HL and has a measurable fringe that scales with photon number, meaning that this class of states is potentially useful for quantum-enhanced interferometry, provided a physical realization can be found. Such a realization is provided in the next section, along with a detailed analysis of the possible performance.

IV. STATE GENERATION

The specific case of $Z = 1$ has been previously examined in Ref. [69], where the proposed experimental design is shown here in Fig. 2(a). By sending each mode of a TMS state to a highly unbalanced beam splitter, a single photon is subtracted from one of the modes. However, before the detection occurs, a third balanced beam splitter is cleverly placed to erase the identifying path information about from which mode the photon came. By detecting exactly one photon on the combined two detection modes, the scheme implements a superposition of performing the subtraction on each mode to create a superposition of the type of states given in Eq. (16), which has the form of

$$\sum_n c_n(|n\rangle_a |n-1\rangle_b + |n-1\rangle_a |n\rangle_b), \tag{31}$$

where the coefficients c_n depend on the strength of the initial TMS state.
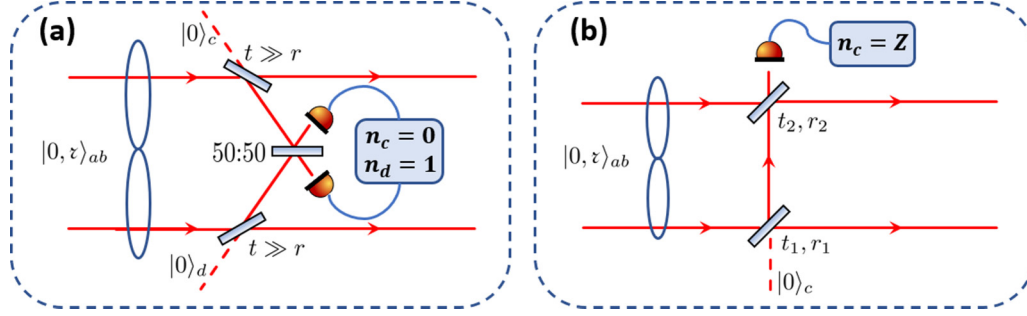
FIG. 2. (a) Scheme using two click detectors to indistinguishably subtract a single photon from two squeezed modes. (b) Simplified version using a single detector that includes the case of coherent single-photon subtraction, but also extends the method to include coherent Z-photon subtraction when a PNR detector is used.

Here, we demonstrate that this state, along with all classes of state given by Eq. (19), can be generated using only a single detector as per the scheme shown in Fig. 2(b). In this implementation, instead of mixing both modes with vacuum to perform the subtraction, an asymmetric scheme is used where only one mode mixes with vacuum while the other is mixed with the siphoned-off portion of the first beam. By tuning the beam-splitter coefficients, it is possible to make a variety of interesting entangled states beyond the scope of Eq. (19), but we will show that utilizing beam splitters with high transmissivity will preserve higher mean photon numbers of the outputs for any given detected number of photons, Z.

The first step of Fig. 2(b) starts with a TMS input state given by

$$|\phi_{\text{in}}\rangle = |0, \nabla\rangle_{ab} |0\rangle_c = \frac{1}{\cosh \nabla} \sum_{n=0}^{\infty} (\tanh \nabla)^n |n\rangle_a |n\rangle_b |0\rangle_c,$$
(32)

where ∇ is the squeezing parameter. The state is sent to the beam splitters each with real reflectivity and transmissivity coefficients such that $t_i^2 + r_i^2 = 1$. Next, the mode c is sent to a PNR detector to measure Z photons and project the remaining modes into the desired state. The output state for the general case is derived in Appendix A and may be useful for engineering interesting two-mode quantum states, but the most desirable case for use in sensitive interferometric measurements occurs when both beam splitters are highly transmissive such that $t \gg r$. This leads to the approximate output state, conditioned on a detection of Z photons, to be

$$|\phi_{\text{out}}\rangle \propto \sum_{n=0}^{\infty} (t^2 \tanh \nabla)^n \sum_{k_{\min}}^{Z} \sqrt{\binom{n}{k}\binom{n}{Z-k}\binom{Z}{k}}$$
$$\times e^{ik\varphi} |n+k-Z\rangle_a |n-k\rangle_b,$$
(33)

where φ is the phase difference between the two input modes to the second beam splitter (t_2, r_2) and $k_{\min} = \text{Max}(0, Z - n)$. This state is simply a superposition of the general class of states given in Eq. (19), where for each $|nn\rangle$ term, the Z photons have been coherently subtracted from both modes in every possible configuration. When φ is set to zero, the coefficients exactly follow the properties specified above in Eq. (27). An important point to note is that the value of n in each input $|nn\rangle$ term is determined by the initial squeezing, but

modified by the beam-splitter transmissivity to yield a new decreased effective squeezing, $\tanh \nabla \rightarrow t^2 \tanh \nabla$. Regardless of the initial squeezing value, this reduction in squeezing means that only values of $t \approx 1$ will allow for useful interferometric measurements as large n is desirable. Cases with t deviating from unity may still work for interferometry applications if a large value of Z is measured; however, this is prohibited by challenges in performing such a large PNR measurement.

V. SQUEEZED INPUT

Numerical simulations were performed using the PYTHON package QUTIP [70] to determine the minimum resolvable fringe from an MZI according to Eq. (29), where the input state was a TMS state that had undergone photon subtraction as per Fig. 2(b).

The results are shown in the top panel of Fig. 3, where Z varies from one to three photons as the initial squeezing is increased, and both beam splitters are taken to be equivalent with reflectivity $r_1 = r_2 \equiv r$. All cases beat the shot-noise limit, but it is clear that decreasing the reflectivity leads to a larger quantum enhancement, and larger values of Z increase the overall phase sensitivity. This behavior may seem odd, as looking at Eq. (30) shows that the overall scaling of the sensitivity is slightly worse as Z increases; however, detecting a larger number of photons acts to increase the mean photon number of the resultant state before the interferometer, and higher-order error terms from the use of beam splitters with nonvanishing reflectivity drop off more quickly with increasing Z. For input states with lower mean photon number, postselecting on a larger Z can actually beat the HL set by the states heralded at smaller Z. However, this comes at the cost of diminishing success rates.

By comparing Figs. 3(a) and 3(b), it is clear that for the relatively large value of $r = 0.2$ the weak beam-splitter approximation employed earlier is no long valid for smaller Z, as the state with $Z = 1$ is only marginally better than the classical case. However, decreasing the reflectivity to $r = 0.1$ suffices to give a quantum advantage that scales when increasing the input energy for all detected values of Z. This highlights the importance of choosing an optimal beam-splitter coefficient that pairs with the desired postselection value, Z, to yield
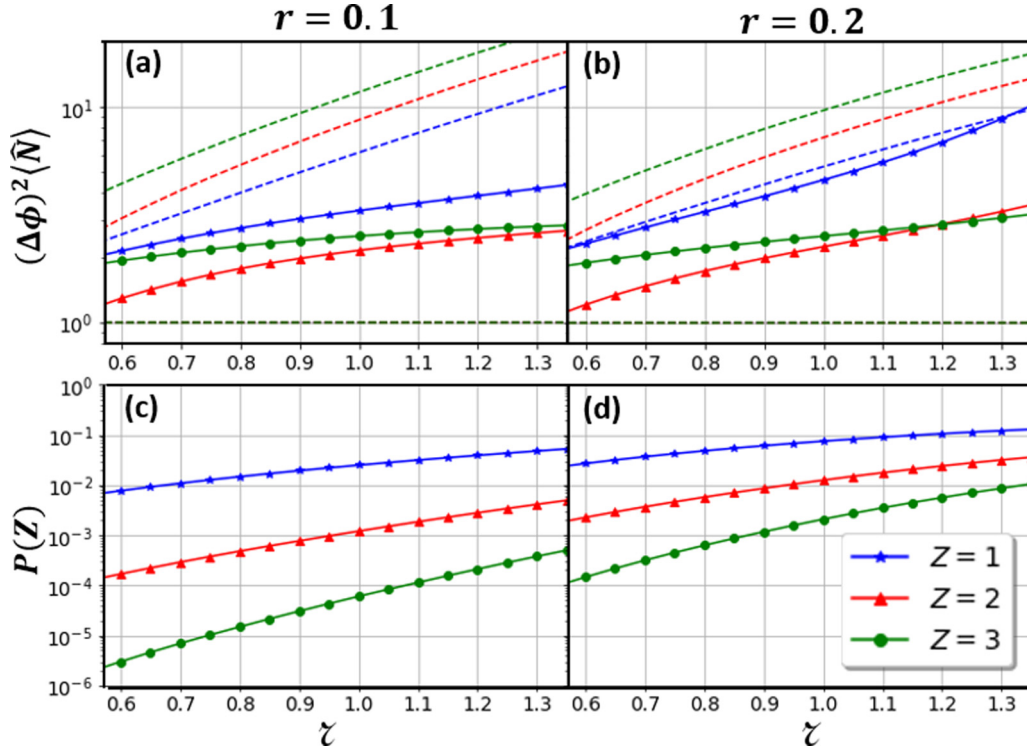
FIG. 3. Minimum phase sensitivity for a photon-subtracted state where a PNR detector has detected Z photons during state generation where beam-splitter reflectivities are (a) $r_1 = r_2 = 0.1$ and (b) $r_1 = r_2 = 0.2$. States are normalized to their respective HL (lower dotted line) with upper dotted lines showing the respective shot-noise levels. Probability to successfully detect Z photons vs input state squeezing for the beam-splitter coefficients (c) $r_1 = r_2 = 0.1$ and (d) $r_1 = r_2 = 0.2$ are also shown.

increased sensitivity while balancing success rates for a given input state.

VI. PRACTICAL CONSIDERATIONS

A. PNR detector loss

In a realistic implementation, one might think that the state generation is highly sensitive to PNR detector efficiency. However, provided any imperfections in the detector are not too drastic, the present scheme is tolerant to this inefficiency. Instead of projecting mode c of the intermediate state following the beam splitters onto an ideal measurement of Z photons, consider a detector positive operator-valued measure (POVM) given by

$$D(Z) = \sum_{l=Z}^{\infty} \binom{l}{Z} \eta^Z (1-\eta)^{l-Z} |l\rangle \langle l|, \qquad (34)$$

where the detector has efficiency η and the device registers a detection of Z photons. The output density matrix will be given by

$$\rho \propto \mathrm{Tr}_c[D_c(Z)(|\psi\rangle \langle \psi|)_{abc}], \qquad (35)$$

where $|\psi\rangle$ is the state following both beam splitters given by Eq. (A4). This leads to

$$\rho \propto \sum_{l=Z}^{\infty} \binom{l}{Z} \eta^Z (1-\eta)^{l-Z} \rho_l, \qquad (36)$$

where ρ_l is the density matrix of the pure state for an l-photon detection given in Eq. (A5). However, taking $r_1 = r_2 \equiv r$ and $r \ll 1$ yields

$$\rho \approx \sum_{l=Z}^{\infty} \binom{l}{Z} \eta^Z (1-\eta)^{l-Z} \left(\frac{r}{t}\right)^{2l} \rho_l' \qquad (37)$$

$$\propto \sum_{l=Z}^{\infty} \binom{l}{Z} \left(\frac{r^2(1-\eta)}{t^2}\right)^l \rho_l', \qquad (38)$$

where $\rho_l' = |\psi_l'\rangle \langle \psi_l'|$ is an unnormalized pure state with

$$|\psi_l'\rangle = \sum_{n=0}^{\infty} \frac{(t^2 \tanh \nabla)^n}{\cosh \nabla} \sum_{k_{\min}}^{l} \sqrt{\binom{n}{k}\binom{n}{l-k}\binom{l}{k}}$$

$$\times e^{ik\varphi} |n+k-l\rangle_a |n-k\rangle_b. \qquad (39)$$

Equation (38) reveals that even for values of η deviating significantly from unity, we have a final state that is approximately pure, i.e., $\rho \approx \rho_Z'$ when $r^2(1-\eta) \ll 1$, since all terms with $l > Z$ in the sum can be neglected. This regime can always be reached by decreasing r until the approximation holds. However, it is important to note that an imperfect detector reduces the success probability of the scheme by a factor of η^Z.

B. Click–no-click detector

In a similar manner to the above discussion, the PNR detector can be safely replaced with a click–no-click detector without ill effect. Since we showed above that the effects of
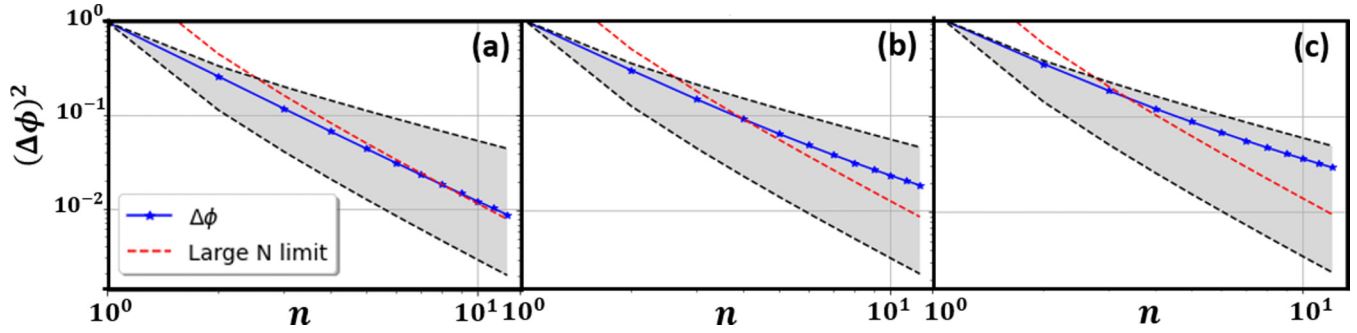
FIG. 4. Minimum phase sensitivity (blue) for a photon-subtracted state with beam-splitter reflectivities $r_1 = r_2 = 0.1$ and input state $|n, n\rangle$, where the PNR detector has been replaced by an ideal click detector. Efficiency η determines the combined transmission of the interferometer and end detector efficiencies and is (a) $\eta = 1$, (b) $\eta = 0.95$, and (c) $\eta = 0.9$. The shot-noise and HL bound the shaded region, and the red dotted line shows the Cramér-Rao bound for the large-N limit with $Z = 1$ given by Eq. (18).

losses during state generation can be considered negligible if the beam-splitter reflectivity is tuned correctly, here we consider an ideal click detector with perfect efficiency. In the case where the detector reads no signal, then the POVM is simply the vacuum as before. In the case of a registered click, the POVM is given by

$$D_{\text{clk}} = \sum_{l=1}^{\infty} |l\rangle \langle l|. \tag{40}$$

Now, the output density matrix is simply a mixture of all possible detected states with $Z \geqslant 1$,

$$\rho \propto \sum_{l=1}^{\infty} P(l)\rho_l, \tag{41}$$

where each of the pure states in the mixture is weighted by the probability of the number of photons that actually went to the detector. Since the quantities of interest are $\langle J_z' \rangle$ and $\Delta J_z'$, we can use the linearity of Eq. (41) along with the results of Appendix B to see that

$$\langle J_z' \rangle = -\sin\phi \sum_{l=1}^{\infty} \text{Tr}[J_x \rho] \tag{42}$$

$$\propto \frac{-\sin\phi}{n} \tag{43}$$

for each component state in the mixture, ρ_l. We also know that the maximum phase sensitivity is achieved about the angle of $\phi = 0$, so the only necessary term from $\Delta J_z'$ is ΔJ_z. Thus, we can find that

$$(\Delta J_z)^2 = \sum_{l=1}^{\infty} \text{Tr}[J_z^2 \rho] \tag{44}$$

$$\overset{(i)}{\leqslant} \sum_{l=1}^{\infty} \frac{l^2}{4}\left(\frac{r}{t}\right)^{2(l-1)}, \tag{45}$$

which leads to a phase sensitivity about $\phi = 0$ of

$$\Delta\phi \propto \frac{1}{n}. \tag{46}$$

These results can be easily understood by realizing that each of the possible pure state components in the mixture that results from the click detection has phase sensitivity scaling

with the HL around the *same* reference phase of $\phi = 0$. Additionally, the high unbalancing of the beam splitters makes the components in the mixture diminish with increasing l.

The results from this section are experimentally significant in that not only does the detector not need the ability to resolve photon numbers, but the imperfect efficiency negligibly degrades the purity of the resultant state, provided that there is precise control in ensuring the beam-splitter reflectivity is small.

C. General OPO output

The general output of an arbitrary twin-beam source, such as obtained from an above-threshold OPO, can be described as a mixture of the form

$$\rho = \sum_{n,n'} \rho_{n,n'} |nn\rangle \langle n'n'|. \tag{47}$$

Despite being a mixture, we show in Appendix C that the indistinguishable multiphoton subtraction protocol also works for this input and leads to a Heisenberg-limited output with phase sensitivity scaling as $\Delta\phi \sim \langle N \rangle^{-1}$. The intuition behind this result follows similar reasons for why a click–no-click detector also fails to ruin Heisenberg-limited sensitivity; although the input is a mixture, each $|n_i, n_i\rangle$ component from the initial twin beam is formed into a superposition with phase sensitivity of $\sim n_i^{-1}$ about the reference angle of $\phi = 0$. Since all of the components of the mixture are Heisenberg limited at the same reference phase, then so is the entirety of the mixture. As such, when considering imperfections such as loss, simulations with the input state $|n, n\rangle$ can be reliably used to gauge the effectiveness of the process for an arbitrary twin-beam source with mean photon number n.

Figure 4 compares the phase sensitivity of a photon-subtracted state with an $|n, n\rangle$ input for the realistic scenario of a heralding PNR detector replaced by a click detector, and when the interferometer has losses. As shown in the previous section, inefficiencies in the click detector channel can be accounted for by choosing a small enough beam-splitter reflectivity, so the click detector here is considered ideal for simplicity. Additionally, if we assume that losses on both interferometer arms are identical, then the losses can be

commuted and combined with detection losses to result in a single overall efficiency of η in each arm [71].

Each plot shows the phase sensitivity along with the large-n limit given by the Cramér-Rao bound for a single photon subtraction given by Eq. (18) (red dotted line). When the beam-splitter reflectivities are small enough for the approximation to apply, as in Fig. 4(a), it can be seen that the phase sensitivity readily follows the Cramér-Rao bound, which scales with the HL up to a constant factor. This constant factor comes from the fact that since each mode in the twin beam has n input photons, the total number of photons in the system is $2n$, leading to a HL of $(2n)^{-1}$; however, the ideal scaling with the single-photon subtracted state goes as n^{-1}. The second and third panels demonstrate that realistic interferometric losses do not drastically reduce the phase sensitivity, such as occurs with states less resilient to loss, such as NOON states. As shown in Fig. 4(b), the slope of the phase sensitivity still scales better than $\langle n \rangle^{-1/2}$ for $\eta = 0.95$, and it is possible to achieve considerably larger overall η in practical experiments with advanced low-loss optical coatings and highly efficient detectors [31]. Figure 4(c), with $\eta = 0.9$, shows how larger losses on the order of $\langle N \rangle^{-1}$ bring the resultant phase sensitivity away from the HL and back to scaling with the shot noise, in agreement with the general result of Escher, de Matos Filho, and Davidovich [28].

VII. DISTINGUISHABLE SUBTRACTION WITHOUT COHERENCE

Thus far we have focused solely on the state we propose, the Z-photon coherently subtracted twin-beam state. However, it is illustrative to compare with the case where Z photons have been distinguishably subtracted from a twin-beam state *without* preserving coherence. One example of this is the case explored previously by Carranza and Gerry [53], where a single photon had been subtracted from each mode of a TMS state. As discussed in Sec. VI, the coherent photon subtraction presented in this article will yield a state with HL sensitivity for any twin-beam correlated photon input, but for the comparison here, we consider the input to be a TMS state and the subtraction process to be ideal with beam-splitter reflectivity $r \to 0$. In this case, the beam-splitter operator can be approximated to first order as

$$U_{\mathrm{BS}} = e^{\theta(a^\dagger b - ab^\dagger)} \approx 1 + \theta(a^\dagger b - ab^\dagger), \quad (48)$$

where $r = \sin\theta \ll 1$. A distinguishable subtraction of z_1 photons in mode a and z_2 photons in mode b transforms the TMS input to

$$
\begin{aligned}
|\phi_{\mathrm{out}}\rangle &\propto {}_c\langle z_1|\, {}_d\langle z_2|(1 + \theta(a^\dagger c - ac^\dagger) \\
&\quad + \theta(b^\dagger d - bd^\dagger)) |0, \nabla\rangle_{ab} |00\rangle_{cd} \\
&\propto \sum_{n=0}^{\infty} \frac{n!(\tanh\nabla)^n}{\sqrt{(n-z_1)!(n-z_2)!}} |n-z_1\rangle_a |n-z_2\rangle_b. \quad (49)
\end{aligned}
$$

Although subtracting photons from the TMS state has the interesting effect of increasing the average photon number of the remaining distribution as noted previously [53,72], each term of the superposition has only one Fock-basis component in each mode. Each term takes the form of $c_{nm} |n\rangle |m\rangle$, which
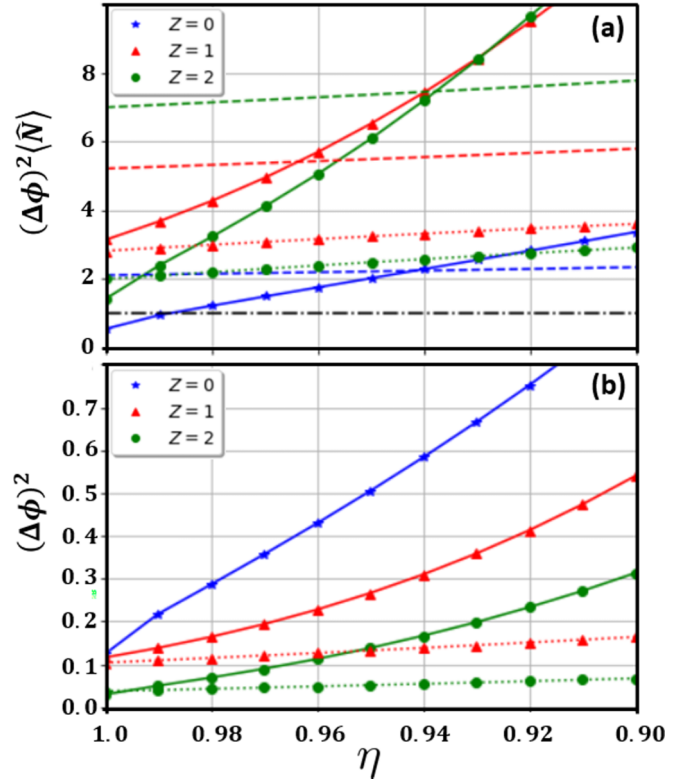

FIG. 5. Minimum phase uncertainties for two-mode squeezed states of squeezing parameter $\nabla = 0.9$ with indistinguishable and distinguishable photon subtraction where Z total photons have been subtracted. Solid lines indicate distinguishable subtraction with $Z = 1$ (red triangles) indicating a photon was subtracted from just one of the two modes and $Z = 2$ (green circles) showing the case where one photon was subtracted from each mode. Dotted lines with markers indicate indistinguishable subtraction between the two modes. Phase sensitivity was calculated using Eq. (50) (parity detection) for cases with distinguishable subtraction and with Eq. (29) (intensity difference detection) for indistinguishable subtraction. The $Z = 0$ curve (blue asterisks) represents the phase sensitivity calculated from parity detection of an unaltered two-mode squeezed state. (a) Phase sensitivity for each state normalized to the Heisenberg limit (black dot-dashed line) with the shot-noise limit for each state shown as an unmarked dashed line of the corresponding color. (b) Raw phase sensitivity comparison of the states.

does not yield an intensity difference fringe scaling with the photon number unless $n \gg m$, which is experimentally unfeasible with photon subtraction due to the low probability of subtracting large numbers of photons. Because of this, states of the form of Eq. (49) will require a different measurement scheme to reach the HL scaling. Introduced by Bollinger *et al.* [22] for trapped ions and later for optical interferometry by Gerry [73], measuring the parity of one output mode, $\Pi_b = (-1)^{b^\dagger b}$, allows for reaching HL sensitivity with these types of input states. With the parity detection scheme, the phase uncertainty becomes

$$(\Delta\phi_\Pi)^2 = \frac{1 - \langle\Pi_b\rangle^2}{|\partial\langle\Pi_b\rangle/\partial\phi|^2}. \quad (50)$$

Optical parity detection is currently an experimental challenge and requires large PNR measurements unless the measured state is of Gaussian nature [74]. Even without this obstacle, the nature of parity predisposes the measurement to be highly susceptible to loss and external noise as the presence or absence of just one photon flips the value of the measurement. This effect is shown in Fig. 5(a), where the phase sensitivity is normalized to the Heisenberg limit (black dot-dashed line) and plotted for several states as the overall interferometric efficiency decreases from $\eta = 1$ to $\eta = 0.90$. Solid curves show the phase sensitivity for the state in Eq. (49) with squeezing parameter $\nabla = 0.9$ where no photons were subtracted (blue), a single photon was subtracted from one of the two modes (red), and the case where one photon was subtracted from each mode (green). The SNL for each curve is shown as a dashed line in the corresponding color. Additionally, Fig. 5 shows the phase sensitivity of the coherently subtracted TMS states with $\nabla = 0.9$, Eq. (33), in fine dotted lines with colors corresponding to the total number of subtracted photons (red for $Z = 1$, green for $Z = 2$). For these states, the phase sensitivity is evaluated with intensity difference detection as per Eq. (29). Note that the state for $Z = 0$ is unchanged from the input TMS state to leading order in r. When there is no loss ($\eta = 1$), it can be seen that all of the states considered have phase sensitivity nearing the HL, and in fact, parity detection with a pure TMS state can actually beat the HL as noted by Anisimov *et al.* [75]. However, even for small losses well below $\langle N \rangle^{-1}$, the states with parity-based detection veer from the HL and quickly become worse than the classical sensitivity bound, unlike the class of states proposed in this article. This behavior is well in line with the results of Ref. [55]. Figure 5(b) shows the phase sensitivity for each state on a true scale without normalization and demonstrates three key points:

(i) Increasing the number of subtracted photons acts to increase the overall mean photon number of the remaining distribution and thus increases phase sensitivity.

(ii) In the absence of loss, both types of states achieve HL sensitivity if the correct measurement scheme is used.

(iii) Finally, for nonzero losses the phase sensitivity of schemes relying on parity detection is quickly degraded whereas the states utilizing an intensity difference measurement retain much of their sensitivity.

VIII. CONCLUSION

We have proposed and studied a nontrivial modification of the twin-beam input for Heisenberg-limited quantum interferometry, which features coherently indistinguishable multiphoton subtraction that leads to a superposition of photon subtractions. This modification brings about a strong fringe signal—absent from the unmodified twin-beam input—while preserving Heisenberg-limited operation. The loss behavior is consistent with what is now well known about Heisenberg-limited interferometry. The experimental implementation should be feasible with state-of-the-art technology, for example using a stable OPO above threshold [20,45,46] and photodetectors with single-photon sensitivity. Detectors with PNR capability may improve the phase sensitivity of the resultant photon-subtracted state by detecting $Z > 1$, but this is not a requirement, and reasonable experimental losses still result in phase sensitivity beating the standard quantum limit. We believe it is possible to operate at no more than 10^6 photons per detection time bin, so as to be compatible with the lowest achievable optical losses and splitting ratios.

APPENDIX A: EXPERIMENTAL STATE DERIVATION

The input state is

$$|\phi_{\text{in}}\rangle = |0, \nabla\rangle_{ab} |0\rangle_c = \frac{1}{\cosh \nabla} \sum_n^\infty (\tanh \nabla)^n |n\rangle_a |n\rangle_b |0\rangle_c . \tag{A1}$$

The overall state is transformed by the beam splitters and projective PNR measurement to become

$$|\phi_{\text{out}}\rangle = {}_c\langle Z| U_{ac} U_{bc} |\phi_{\text{in}}\rangle , \tag{A2}$$

where $U_{bc} = \exp[\theta_1(bc^\dagger - b^\dagger c)]$, and $U_{ac} = \exp[\theta_2(ac^\dagger e^{-i\varphi} - a^\dagger c e^{i\varphi})]$ to allow for an additional phase of φ between mode a and the reflected mode c from the first beam splitter, where reflectivities and transmissivities $r_i = \sin \theta_i$, $t_i = \cos \theta_i$. Note that the second beam-splitter operation, U_{ac}, will act between mode a and the *transformed* mode c from the output of the first beam-splitter operation. With this in mind, the first beam splitter transforms the input state to

$$U_{bc} |\phi_{\text{in}}\rangle = \sum_n^\infty \frac{(\tanh \nabla)^n}{\sqrt{n!} \cosh \nabla} U_{bc} b^{\dagger n} U_{bc}^\dagger |n\rangle_a |0\rangle_b |0\rangle_c$$

$$= \sum_n^\infty \frac{(\tanh \nabla)^n}{\sqrt{n!} \cosh \nabla} (t_1 b^\dagger + r_1 c^\dagger)^n |n\rangle_a |0\rangle_b |0\rangle_c = \sum_n^\infty \frac{(\tanh \nabla)^n}{n! \cosh \nabla} \sum_k^n \binom{n}{k} t_1^k r_1^{n-k} a^{\dagger n} b^{\dagger k} c^{\dagger n-k} |0\rangle_a |0\rangle_b |0\rangle_c . \tag{A3}$$

Now, applying the second beam-splitter yields the state

$$\sum_n^\infty \frac{(\tanh \nabla)^n}{n! \cosh \nabla} \sum_k^n \binom{n}{k} t_1^k r_1^{n-k} b^{\dagger k} (t_2 a^\dagger + e^{i\varphi} r_2 c^\dagger)^n (t_2 c^\dagger - e^{-i\varphi} r_2 a^\dagger)^{n-k} |0\rangle_{abc}$$

$$= \sum_n^\infty \frac{(-r_1 r_2^2 \tanh \nabla)^n}{n! \cosh \nabla} \sum_k^n \binom{n}{k} \left(\frac{t_1}{r_1 r_2}\right)^k b^{\dagger k} \sum_j^n \binom{n}{j} \left(\frac{t_2}{r_2}\right)^j$$

$$\times \sum_m^{n-k} \binom{n-k}{m} (-1)^{m+k} \left(\frac{t_2}{r_2}\right)^m (e^{i\varphi})^{k+m-j} a^{\dagger j+n-k-m} c^{\dagger n-j+m} |0\rangle_{abc}. \tag{A4}$$

Projecting output mode c onto the PNR detection event of Z photons means that the only terms in the above sums that survive occur when $j = n + m - Z$. It is also important to note that the maximum value of j is n, so the remaining sum over m goes from zero to $m_{\max} = \text{Min}(n-k, Z)$. These substitutions lead to

$$|\phi_Z\rangle = \frac{r_2^Z \sqrt{Z!}}{t_2^Z \cosh \nabla} \sum_{n=0}^\infty (-t_2 r_1 r_2 e^{-i\varphi} \tanh \nabla)^n \sum_{k=0}^n \frac{\sqrt{(2n-k-Z)!}}{\sqrt{k!}} \left(\frac{-e^{i\varphi} t_1}{r_1 r_2}\right)^k$$

$$\times \sum_{m=0}^{m_{\max}} \binom{n}{n+m-Z} \left(\frac{t_2}{r_2}\right)^{2m} \frac{(-1)^m}{m!(n-k-m)!} |2n-k-Z\rangle_a |k\rangle_b$$

$$\propto \sum_{n=0}^\infty c_n \sum_{k=k_{min}}^n d_{n,k} |n+k-Z\rangle_a |n-k\rangle_b, \tag{A5}$$

where $k_{\min} = \text{Max}(0, Z-n)$, $c_n = (t_1 t_2 \tanh \nabla)^n$, and the coefficient $d_{n,k}$ is

$$d_{n,k} = \frac{\sqrt{(n+k-Z)!}}{\sqrt{(n-k)!}} \left(\frac{r_1 r_2}{-e^{i\varphi} t_1}\right)^k \sum_{m=0}^{\text{Min}(Z,k)} \binom{n}{n+m-Z} \left(\frac{t_2}{r_2}\right)^{2m} \frac{(-1)^m}{m!(k-m)!}. \tag{A6}$$

The form of the general case in Eq. (A5) shows that, after all is said and done, we have a superposition over n of two-mode superpositions that are desirable for quantum enhanced interferometry, where the c_n terms depend on a new effective squeezing, which is reduced from the original value by the transmissivity of the two beam splitters. The success probability to create this state after a given Z PNR detection is given by

$$P(Z) = \frac{Z!}{(\cosh \nabla)^2} \left(\frac{r_2}{t_2}\right)^{2Z} \sum_{n=0}^\infty \sum_{k=k_{\min}}^n c_n^2 d_{n,k}^2 \tag{A7}$$

1. Highly unbalanced beam splitters

If we consider the case where both beam splitters are identical and highly transmissive with $r_1 = r_2 \equiv r$ and $r \ll 1$, then examining Eq. (A6) shows that only the term with $m = k$ contributes to the coefficient d_n to leading order. Furthermore, since the sum over m is truncated at $m_{\max} = \text{Min}(k, Z)$, the sum over k in Eq. (A5) can be effectively truncated at Z to the same order of approximation. The output state then becomes

$$|\phi_Z\rangle \propto \sum_{n=0}^\infty (t^2 \tanh \nabla)^n \sum_{k_{\min}}^Z \sqrt{\binom{n}{k}\binom{n}{Z-k}\binom{Z}{k}} e^{ik\varphi} |n+k-Z\rangle_a |n-k\rangle_b, \tag{A8}$$

with an approximate success probability of

$$P(Z) \approx \frac{r^{2Z}}{(\cosh \nabla)^2} \sum_{n=0}^\infty (1-2nr^2)(\tanh \nabla)^{2n} \sum_{k_{\min}}^Z \binom{n}{k}\binom{n}{Z-k}\binom{Z}{k}. \tag{A9}$$

2. Coefficients

Here we verify several properties of the coefficients of the experimental state. In the case of a highly unbalanced beam splitter, then for a given n, the experimental state takes the form of Eq. (19) with coefficients having the form shown in Eq. (A8) to be

$$c_k \propto \sqrt{\binom{n}{k}\binom{n}{Z-k}\binom{Z}{k}} e^{ik\varphi}, \tag{A10}$$

where all c_k have the same proportionality constant from normalization. Setting $\varphi = 0$ ensures that all c_k are real. When writing the state in the Schwinger representation, these coefficients become

$$c_m \propto \sqrt{\binom{n}{m+s}\binom{n}{s-m}\binom{2s}{m+s}}, \tag{A11}$$

where $s = \frac{Z}{2}$ and $m = k - s$, from which it is clear to see that

$$c_m = c_{-m}. \tag{A12}$$

Now, how do neighboring coefficients relate? Calculating the ratio between neighbors yields

$$\frac{c_{m+1}}{c_m} = \frac{s-m}{s+m+1}\left(\frac{n-s-m}{n-s+m+1}\right)^{1/2}, \tag{A13}$$

which leads to the bounds of

$$\frac{1}{2s} \overset{(i)}{\leqslant} \frac{c_{m+1}}{c_m} \overset{(i)}{\leqslant} 2s, \tag{A14}$$

where "(i)" denotes the use of the approximation that $n \gg s$. This ratio is useful when calculating terms that appear in expectation values, and can be used to determine a bound on the sum of all pairs of neighboring coefficients to be

$$\frac{1}{2s} \overset{(i)}{\leqslant} \sum_{m=-s}^{s-1} c_m c_{m+1} \leqslant 1, \tag{A15}$$

where the upper bound can be derived from the Cauchy-Schwarz inequality. Similarly, the ratio between next-neighboring coefficients has the bound

$$\frac{c_{m+2}}{c_m} \overset{(i)}{\geqslant} \frac{1}{s(2s-1)}, \tag{A16}$$

which leads to bounding the sum of next-nearest-neighboring coefficients to be

$$\frac{1}{2s^2 - s} \overset{(i)}{\leqslant} \sum_{m=-s}^{s-2} c_m c_{m+2} \leqslant 1. \tag{A17}$$

APPENDIX B: GENERAL MULTIPHOTON SUBTRACTED STATE

Here we derive the Fisher information for the general case of the state given by Eq. (19). All of the relevant terms are

$$\langle a^\dagger b \rangle = \sum_{k=0}^{Z-1} c_k c_{k+1}^* \sqrt{(n-k)(n-Z+k+1)},$$

$$\langle ab^\dagger \rangle = \sum_{k=0}^{Z-1} c_k^* c_{k+1} \sqrt{(n-k+1)(n-Z+k)},$$

$$\langle a^\dagger a b b^\dagger \rangle = \sum_{k=0}^{Z} |c_k|^2 (n-Z+k)(n-k+1)),$$

$$\langle a a^\dagger b^\dagger b \rangle = \sum_{k=0}^{Z} |c_k|^2 (n-Z+k+1)(n-k)),$$

$$\langle a^\dagger a^\dagger b b \rangle = \sum_{k=0}^{Z-2} c_k c_{k+2}^* \sqrt{(n-k)(n-k-1)(n-Z+k+1)(n-Z+k+2)},$$

$$\langle a a b^\dagger b^\dagger \rangle = \sum_{k=0}^{Z-2} c_k^* c_{k+2} \sqrt{(n-k+1)(n-k+2)(n-Z+k)(n-Z+k-1)}.$$

If we take a case where the number of photons removed from the state is small compared to the total, i.e., $n \gg Z$, then, denoting the use of this approximation as (i), the Fisher information is

$$\mathcal{F} \overset{(i)}{=} 2\sum_{k=0}^{Z} n^2 |c_k|^2 - \sum_{k=0}^{Z-2} n^2(c_k c_{k+2}^* + c_k^* c_{k=2}) + \left(\sum_{k=0}^{Z-1} n c_k c_{k+1}^*\right)^2$$

$$+ \left(\sum_{k=0}^{Z-1} n c_k^* c_{k+1} \right)^2 - \sum_{k=0}^{Z-1} \sum_{k'=0}^{Z-1} n^2 (c_k c_{k+1}^* c_{k'}^* c_{k'+1} + c_k^* c_{k+1} c_{k'} c_{k'+1}^*). \tag{B1}$$

If we now make assumption (ii) that all of the coefficients are the same, $c_k = \frac{1}{\sqrt{Z}}$, then

$$\mathcal{F} \overset{\text{(i,ii)}}{=} \frac{4n^2}{Z}, \tag{B2}$$

so the Cramér-Rao inequality leads to

$$(\Delta \phi_d)^2 \geqslant \frac{Z}{N^2}, \tag{B3}$$

where $N = 2n - Z$.

MZI fringe and phase sensitivity

Using the Schwinger representation to determine the observables when the general Z-subtracted state from Eq. (26) is input into a MZI, we start by finding the expectation value of J_x and J_z. We find that

$$\langle J_z \rangle = 0,$$

$$\langle J_x \rangle = \frac{1}{2} \sum_{m=1-s}^{s} c_{m-1}^* c_m \sqrt{(j+m)(j-m+1)} + \frac{1}{2} \sum_{m=-s}^{s-1} c_{m+1}^* c_m \sqrt{(j-m)(j+m+1)}$$

$$= \sum_{m=-s}^{s-1} c_{m+1} c_m \sqrt{(j-m)(j+m+1)} \overset{\text{(i)}}{=} j \sum_{m=-s}^{s-1} c_{m+1} c_m, \tag{B4}$$

where we have used that all $c_m \in \mathbb{R}$, $c_m = c_{-m}$, and have used approximation (i) that $j \gg s$. From here, we can estimate the value of the remaining sum by making use of the bounds on $\frac{c_{m+1}}{c_m}$, denoted by (ii), for all of the coefficients derived in Appendix A 2. This leads to the result that

$$\frac{j}{2s} \overset{\text{(i,ii)}}{\leqslant} \langle J_x \rangle \overset{\text{(i)}}{\leqslant} j. \tag{B5}$$

The observable fringe is given by the expectation value of $2J_z$ at the output, where

$$|\langle J_z' \rangle| = |\cos\phi \langle J_z \rangle - \sin\phi \langle J_x \rangle| \frac{j}{2s} |\sin\phi| \overset{\text{(i,ii)}}{\leqslant} |\langle J_z' \rangle| \overset{\text{(i)}}{\leqslant} j |\sin\phi|. \tag{B6}$$

The end result above shows that the measurable fringe scales with the mean photon number of the state. When calculating $\Delta\phi$, the Heisenberg transformations yield

$$\frac{\partial d}{\partial d\phi} \langle J_z' \rangle = -\sin\phi \langle Jz \rangle - \cos\phi \langle Jx \rangle, \tag{B7}$$

$$(\Delta J_z')^2 = (\cos\phi \Delta J_z)^2 + (\sin\phi \Delta J_x)^2 - \sin\phi \cos\phi (\langle \{J_z, J_x\} \rangle - 2\langle Jz \rangle \langle Jx \rangle). \tag{B8}$$

Deriving the quantities individually, we have

$$(\Delta J_z)^2 = \langle J_z^2 \rangle = \sum_{m=-s}^{s} m^2 |c_m|^2 < s^2, \tag{B9}$$

where the inequality is obtained by replacing all m^2 with the maximum value of s^2. We also find that

$$\langle J_x^2 \rangle = \frac{1}{4} \langle J_+^2 + J_-^2 + 2(J^2 - J_z^2) \rangle$$

$$= \frac{1}{2} \sum_{m=-s}^{s} |c_m|^2 (j^2 + j - m^2) + \frac{1}{2} \sum_{m=-s}^{s-2} c_m c_{m+2} \sqrt{(j+m+2)(j-m-1)(j+m+1)(j-m)}$$

$$\overset{\text{(i)}}{=} \frac{j(j+1)}{2} - \frac{s^2}{2} + \frac{1}{2}(j^2 - s^2) \sum_{m=-s}^{s-2} c_m c_{m+2},$$

$$\frac{j^2}{2} \left(1 + \frac{1}{s(2s+1)} \right) + \frac{j}{2} \overset{\text{(i,ii)}}{\leqslant} \langle J_x^2 \rangle \overset{\text{(i)}}{\leqslant} 1, \tag{B10}$$

where the final inequality is obtained by bounding the sum in the second-to-last line with the ratio of next-nearest-neighboring coefficients   derived   in Appendix A 2. This leads to the variance

$$(\Delta J_x)^2 \sim O(j^2).$$ (B11)

The other necessary terms are

$$\langle \{J_z, J_x\} \rangle = \sum_{m=-s}^{s-1} (2m+1) c_{m+1} c_m \sqrt{(j-m)(j+m+1)} \approx \langle J_x \rangle,$$ (B12)

$$2\langle Jz \rangle \langle Jx \rangle = 0,$$ (B13)

which when combined with Eqs. (B6), (B9), and (B11) lead to an overall value for the phase difference estimator given by Eq. (29) to be

$$(\Delta \phi)^2 \overset{(i)}{\leqslant} \frac{(s\cos\phi)^2 + (\Delta J_x \sin\phi)^2 + \sin\phi\cos\phi\langle J_x \rangle}{(\frac{j}{2s}\cos\phi)^2}.$$ (B14)

This takes on a minimum value when $\phi = 0$ to yield the upper bound

$$\Delta\phi_{\min} \overset{(i,ii)}{\leqslant} \frac{2s^2}{j},$$ (B15)

which scales with the HL up to a constant factor. By taking the upper limit of $\langle J_x \rangle$ from Eq. (B5), the lower bound on $\Delta\phi$ when $\phi = 0$ is

$$\frac{\sqrt{s}}{j} \overset{(i,ii)}{\leqslant} \Delta\phi_{\min}.$$ (B16)

APPENDIX C: PHASE SENSITIVITY FOR A GENERAL TWIN-BEAM INPUT

In this section, we show that our photon subtraction protocol also works for the most general twin-beam statistical mixture, e.g., as produced by an OPO above threshold. The density operator in the Fock basis is given by

$$\rho_{ab} = \sum_{n,n'} \rho_{n,n'} |nn\rangle \langle n'n'|.$$ (C1)

The two beam-splitter operations are given by

$$U_{ac'} U_{bc} = \exp[\theta_2 (a^\dagger c' - ac'^\dagger)] \exp[\theta_1 (b^\dagger c - bc^\dagger)] = \sum_{j,k} \frac{\theta_1^k \theta_2^j}{j!k!} (a^\dagger c' - ac'^\dagger)^j (b^\dagger - bc^\dagger)^k,$$ (C2)

where $c' = c\cos\theta_1 - b\sin\theta_1$ is the transformed vacuum mode from the first beam-splitter input. Because the input state, ρ_{ab}, consists solely of vacuum in the input mode c, and we are postselecting the transformed mode c on a detection of Z photons, we need only consider terms of the form $c^x c^{\dagger(x+Z)}$ and $c^{\dagger(x+Z)} c^x$. To further simplify, we can assume the highly unbalanced beam-splitter regime, where both $\theta_1 \ll 1$ and $\theta_2 \ll 1$, in which case we need only consider terms with $c^{\dagger Z}$. Thus, to leading order in θ, we have $j + k = Z$ and

$$U_{ac'} U_{bc} \approx \sum_{k=0}^{Z} \frac{r_1^k r_2^{Z-k}}{k!(Z-k!)} (-at_1)^{Z-k} (-b)^k c^{\dagger Z},$$ (C3)

where $r_1 = \sin\theta_1 \approx \theta_1$ and $r_2 = \sin\theta_2 \approx \theta_2$. Sending the twin-beam input through the unbalanced beam splitters and detecting Z photons in mode c leads to

$$\rho_{\text{out}} = \text{Tr}_c[(|Z\rangle\langle Z|)_c U_{ac'} U_{bc} \rho_{ab} \otimes |0\rangle\langle 0| U_{bc}^\dagger U_{ac'}^\dagger]$$ (C4)

$$= \text{Tr}_c\left[(|Z\rangle\langle Z|)_c \sum_{k,k'}^{Z} \frac{r_1^{k+k'} r_2^{2Z-k-k'} t_1^{2Z-k-k'}}{k!k'!(Z-k)!(Z-k')!} \sum_{n,n'}^{\infty} \rho_{n,n'} a^{Z-k} b^k c^{\dagger Z} |n,n,0\rangle\langle n',n',0| a^{\dagger(Z-k')} b^{\dagger k'} c^Z \right]$$ (C5)

$$\propto (r_2 t_1)^{2Z} \sum_{n,n'}^{\infty} \rho_{n,n'} \sum_{k,k'}^{Z} C_{k,k'} |n-Z+k, n-k\rangle\langle n'-Z+k', n'-k'|,$$ (C6)

where $C_{n,n'}$ contains all of the remaining binomial coefficients,

$$C_{n,n'} = \left[\binom{n}{k}\binom{Z}{k}\binom{n}{Z-k}\binom{n'}{k'}\binom{Z}{k'}\binom{n'}{Z-k'}\right]^{1/2}\left(\frac{r_1}{t_1 r_2}\right)^{k+k'}. \tag{C7}$$

Writing the output in the Schwinger representation, we have

$$\rho_{\text{out}} = \sum_{j,j'}^{\infty} \rho_{j,j'} \sum_{m,m'=-s}^{s} C'_{m,m'}|j,m\rangle\langle j',m'|, \tag{C8}$$

where $s = \frac{Z}{2}$. From here, the calculations for the Schwinger operators follow the form of Appendix B for each of the superpositions within the mixture, leading to the finding that, about the interferometric phase $\phi = 0$, we have that $(\Delta J'_z)^2 \leqslant s^2$. Additionally, following the arguments of Appendix A 2, we find that $\langle J_x \rangle \geqslant \frac{j_{\text{avg}}}{2s}$, where j_{avg} is the average value of j in the statistical mixture. These values lead to the determination that about $\phi = 0$,

$$\Delta\phi = \frac{(\Delta J'_z)}{\left|\frac{\partial}{\partial\phi}\langle J'_z\rangle\right|}\Big|_{\phi=0} \overset{\text{(i,ii)}}{\leqslant} \frac{2s^2}{j_{\text{avg}}}, \tag{C9}$$

and hence the general twin-beam source is sufficient to achieve phase-sensitivity scaling proportionally with the HL.

[1] C. M. Caves, Phys. Rev. Lett. **45**, 75 (1980).

[2] The SNL is often called the "standard quantum limit." However, the latter was initially defined with a different meaning, in order to address the optimum error of quantum measurements in the presence of back-action, such as radiation pressure on interferometer mirrors [3,4].

[3] C. M. Caves, K. S. Thorne, R. W. P. Drever, V. D. Sandberg, and M. Zimmermann, Rev. Mod. Phys. **52**, 341 (1980).

[4] V. B. Braginsky and F. Y. Khalili, *Quantum Measurement*, edited by K. S. Thorne (Cambridge University Press, Cambridge, UK, 1992).

[5] From the number-phase Heisenberg inequality $\Delta N \Delta\phi \geqslant 1/2$, easily derived from the energy-time inequality [6].

[6] J.-M. Lévy-Leblond and F. Balibar, *Quantics: Rudiments of Quantum Physics* (North-Holland, Amsterdam, 1990).

[7] R. Demkowicz-Dobrzański, M. Jarzyna, and J. Kołodyński, in *Progress in Optics* (Elsevier, Amsterdam, 2015), Chap. 4, pp. 345–435.

[8] C. M. Caves, Phys. Rev. D **23**, 1693 (1981).

[9] M. D. Lang and C. M. Caves, Phys. Rev. Lett. **111**, 173601 (2013).

[10] P. Grangier, R. E. Slusher, B. Yurke, and A. LaPorta, Phys. Rev. Lett. **59**, 2153 (1987).

[11] M. Xiao, L. A. Wu, and H. J. Kimble, Phys. Rev. Lett. **59**, 278 (1987).

[12] J. Abadie *et al.* (The LIGO Collaboration), Nat. Phys. **7**, 962 (2011).

[13] J. Aasi *et al.* (The LIGO Collaboration), Nat. Photonics **7**, 613 (2013).

[14] B. Yurke, S. L. McCall, and J. R. Klauder, Phys. Rev. A **33**, 4033 (1986).

[15] A. Luis and L. Sánchez-Soto, Prog. Opt. **41**, 421 (2000).

[16] M. J. Holland and K. Burnett, Phys. Rev. Lett. **71**, 1355 (1993).

[17] P. Bouyer and M. A. Kasevich, Phys. Rev. A **56**, R1083(R) (1997).

[18] T. Kim, O. Pfister, M. J. Holland, J. Noh, and J. L. Hall, Phys. Rev. A **57**, 4004 (1998).

[19] J. P. Dowling, Phys. Rev. A **57**, 4736 (1998).

[20] S. Feng and O. Pfister, Phys. Rev. Lett. **92**, 203601 (2004).

[21] S. Feng and O. Pfister, Opt. Lett. **29**, 2800 (2004).

[22] J. J. Bollinger, W. M. Itano, D. J. Wineland, and D. J. Heinzen, Phys. Rev. A **54**, R4649(R) (1996).

[23] A. N. Boto, P. Kok, D. S. Abrams, S. L. Braunstein, C. P. Williams, and J. P. Dowling, Phys. Rev. Lett. **85**, 2733 (2000).

[24] M. W. Mitchell, J. S. Lundeen, and A. M. Steinberg, Nature **429**, 161 (2004).

[25] P. Walther, J.-W. Pan, M. Aspelmeyer, R. Ursin, S. Gasparoni, and A. Zeilinger, Nature **429**, 158 (2004).

[26] I. Afek, O. Ambar, and Y. Silberberg, Science **328**, 879 (2010).

[27] M. D. Lang and C. M. Caves, Phys. Rev. A **90**, 025802 (2014).

[28] B. M. Escher, R. L. de Matos Filho, and L. Davidovich, Nat. Phys. **7**, 406 (2011).

[29] R. C. Pooser and O. Pfister, Phys. Rev. A **69**, 043616 (2004).

[30] U. Dorner, R. Demkowicz-Dobrzanski, B. J. Smith, J. S. Lundeen, W. Wasilewski, K. Banaszek, and I. A. Walmsley, Phys. Rev. Lett. **102**, 040403 (2009).

[31] J. Aasi, B. Abbott, R. Abbott, T. Abbott, M. Abernathy, K. Ackley, C. Adams, T. Adams, P. Addesso, R. Adhikari *et al.*, Classical Quantum Gravity **32**, 115012 (2015).

[32] R. W. P. Drever, J. L. Hall, F. V. Kowalski, J. Hough, G. M. Ford, A. J. Munley, and H. Ward, Appl. Phys. B **31**, 97 (1983).

[33] H. Vahlbruch, M. Mehmet, K. Danzmann, and R. Schnabel, Phys. Rev. Lett. **117**, 110801 (2016).

[34] H. Vahlbruch, S. Chelkowski, B. Hage, A. Franzen, K. Danzmann, and R. Schnabel, Phys. Rev. Lett. **97**, 011101 (2006).

[35] M. Tse, H. Yu, N. Kijbunchoo, A. Fernandez-Galiana, P. Dupej, L. Barsotti, C. Blair, D. Brown, S. Dwyer, A. Effler *et al.*, Phys. Rev. Lett. **123**, 231107 (2019).

[36] F. Acernese, M. Agathos, L. Aiello, A. Allocca, A. Amato, S. Ansoldi, S. Antier, M. Arène, N. Arnaud, S. Ascenzi *et al.*, Phys. Rev. Lett. **123**, 231108 (2019).

[37] H. Grote, K. Danzmann, K. L. Dooley, R. Schnabel, J. Slutsky, and H. Vahlbruch, Phys. Rev. Lett. **110**, 181101 (2013).

[38] L. McCuller, C. Whittle, D. Ganapathy, K. Komori, M. Tse, A. Fernandez-Galiana, L. Barsotti, P. Fritschel, M. MacInnis, F. Matichard *et al.*, Phys. Rev. Lett. **124**, 171102 (2020).

[39] A. Heidmann, R. J. Horowicz, S. Reynaud, E. Giacobino, C. Fabre, and G. Camy, Phys. Rev. Lett. **59**, 2555 (1987).

[40] J. Mertz, T. Debuisschert, A. Heidmann, C. Fabre, and E. Giacobino, Opt. Lett. **16**, 1234 (1991).

[41] J. Laurat, L. Longchambon, C. Fabre, and T. Coudreau, Opt. Lett. **30**, 1177 (2005).

[42] This is the most general mixture for which $\langle N_a - N_b \rangle = 0$ and $\Delta(N_a - N_b) = 0$.

[43] R. A. Campos, B. E. A. Saleh, and M. C. Teich, Phys. Rev. A **40**, 1371 (1989).

[44] C. K. Hong, Z. Y. Ou, and L. Mandel, Phys. Rev. Lett. **59**, 2044 (1987).

[45] J. Jing, S. Feng, R. Bloomer, and O. Pfister, Phys. Rev. A **74**, 041804(R) (2006).

[46] M. Pysher, Y. Miwa, R. Shahrokhshahi, and O. Pfister, Opt. Express **18**, 27858 (2010).

[47] C. You, M. Hong, P. Bierhorst, A. E. Lita, S. Glancy, S. Kolthammer, E. Knill, S. W. Nam, R. P. Mirin, O. S. Magana-Loaiza *et al.*, arXiv:2011.02454.

[48] J. J. Snyder, E. Giacobino, C. Fabre, A. Heidmann, and M. Ducloy, J. Opt. Soc. Am. B **7**, 2132 (1990).

[49] G. S. Thekkadath, M. E. Mycroft, B. A. Bell, C. G. Wade, A. Eckstein, D. S. Phillips, R. B. Patel, A. Buraczewski, A. E. Lita, T. Gerrits *et al.*, npj Quantum Inf. **6**, 89 (2020).

[50] M. Kacprowicz, R. Demkowicz-Dobrzański, W. Wasilewski, K. Banaszek, and I. Walmsley, Nat. Photonics **4**, 357 (2010).

[51] A. E. Ulanov, I. A. Fedorov, D. Sychev, P. Grangier, and A. Lvovsky, Nat. Commun. **7**, 11925 (2016).

[52] R. Birrittella and C. C. Gerry, J. Opt. Soc. Am. B **31**, 586 (2014).

[53] R. Carranza and C. C. Gerry, J. Opt. Soc. Am. B **29**, 2581 (2012).

[54] U. Leonhardt, Phys. Rev. A **49**, 1231 (1994).

[55] D. Li, C.-H. Yuan, Y. Yao, W. Jiang, M. Li, and W. Zhang, J. Opt. Soc. Am. B **35**, 1080 (2018).

[56] A. M. Marino, N. V. Corzo Trejo, and P. D. Lett, Phys. Rev. A **86**, 023844 (2012).

[57] S. Adhikari, N. Bhusal, C. You, H. Lee, and J. P. Dowling, OSA Continuum **1**, 438 (2018).

[58] B. E. Anderson, B. L. Schmittberger, P. Gupta, K. M. Jones, and P. D. Lett, Phys. Rev. A **95**, 063843 (2017).

[59] P. Gupta, B. L. Schmittberger, B. E. Anderson, K. M. Jones, and P. D. Lett, Opt. Express **26**, 391 (2018).

[60] J.-D. Zhang, C.-F. Jin, Z.-J. Zhang, L.-Z. Cen, J.-Y. Hu, and Y. Zhao, Opt. Express **26**, 33080 (2018).

[61] C. M. Caves, Adv. Quantum Technol. **3**, 1900138 (2020).

[62] G. Frascella, S. Agne, F. Y. Khalili, and M. V. Chekhova, arXiv:2005.08843.

[63] H. Cramér, *Mathematical Methods of Statistics*, Vol. 43 (Princeton University Press, Princeton, NJ, 1999).

[64] C. R. Rao, in *Breakthroughs in Statistics* (Springer, Berlin, 1992), pp. 235–247.

[65] C. W. Helstrom, J. Stat. Phys. **1**, 231 (1969).

[66] M. Jarzyna and R. Demkowicz-Dobrzański, Phys. Rev. A **85**, 011801(R) (2012).

[67] J. Schwinger, U.S. Atomic Energy Commission Report No. NYO-3071 (1952), reprinted in *Quantum Theory of Angular Momentum*, edited by L. C. Biedenharn and H. van Dam (Academic Press, New York, 1965), pp. 229–279.

[68] S. L. Braunstein and C. M. Caves, Phys. Rev. Lett. **72**, 3439 (1994).

[69] H. F. Hofmann, Phys. Rev. A **74**, 013808 (2006).

[70] J. R. Johansson, P. D. Nation, and F. Nori, Comput. Phys. Commun. **183**, 1760 (2012).

[71] C. Oh, S.-Y. Lee, H. Nha, and H. Jeong, Phys. Rev. A **96**, 062304 (2017).

[72] M. S. Kim, E. Park, P. L. Knight, and H. Jeong, Phys. Rev. A **71**, 043805 (2005).

[73] C. C. Gerry, Phys. Rev. A **61**, 043811 (2000).

[74] W. N. Plick, P. M. Anisimov, J. P. Dowling, H. Lee, and G. S. Agarwal, New J. Phys. **12**, 113025 (2010).

[75] P. M. Anisimov, G. M. Raterman, A. Chiruvelli, W. N. Plick, S. D. Huver, H. Lee, and J. P. Dowling, Phys. Rev. Lett. **104**, 103602 (2010).